eXPRESS Polymer Letters Vol.5, No.6 (2011) 545–554
Available online at www.expresspolymlett.com
DOI: 10.3144/expresspolymlett.2011.53

Rapid biomimetic mineralization of chitosan scaffolds with a precursor sacrificed method in ethanol/water mixed solution

L. H. Li[1,2], *M. Y. Zhao*[1,2], *S. Ding*[1,2], *C. R. Zhou*[1,2*]

[1]Department of Materials Science and Engineering, Jinan University, Guangzhou, 510630, China
[2]Engineering Research Center of Artificial Organs and Materials, Ministry of Education, Guangzhou, 510630, China

Received 2 November 2010; accepted in revised form 30 December 2010

Abstract. Biomimetic mineralization was performed on a large scale by a rapid and efficient approach. Chitosan scaffolds were placed in a mixed solution of urea, ethanol and distilled water, followed by the introduction of dibasic sodium phosphate (0.1M) and calcium chloride (0.1M) with the molar ratio of 1.67. These mixed solvents was then adjusted to weakly alkaline by adding sodium hydroxide solution. Finally the reaction mixture was sealed and kept at 80ºC for predetermined time. The composition and morphology of the apatite and the hybrid scaffolds were investigated by X-ray diffraction (XRD), transmission electron microscopy (TEM), Fourier Transform Infrared spectroscopy (FTIR) and environmental scanning electron microscopy (ESEM). The mechanism of nucleation and growth of crystals was discussed as well. The results revealed that chitosan scaffolds improved the crystallinity of hydroxyapatite (HAP) crystals. With the extension of mineralization time, the mineral layers on the outer surface and inner section of chitosan scaffolds increased as well. Furthermore, the compressive strength and modulus of the HAP-chitosan scaffolds biocomposites increased to 0.55±0.003 and 29.29±1.25 MPa respectively. Such one-pot approach may be extended to the mineralization of other materials and will have a broad application in the future.

Keywords: *biocomposites, mineralization, chitosan, hydroxyapatite*

1. Introduction

Bone is considered as a nanocomposite of minerals and proteins. Recently nano-sized hydroxyapatite (HAP) and its composites with polymers have been investigated with fascination and demonstrated a good impact on cell–biomaterial interaction [1, 2]. However, the migration of the nano HAP particles from the implanted site into surrounding tissues might cause damage to healthy tissues. Current advances in molecular biomimetics suggest that a biomineral-inspired approach may be of value in new classes of biomaterials [3, 4]. This approach is based primarily on the idea of macromolecules as templates to control inorganic crystal formation, and seeks to reproduce the nanoscopic and hierarchical structures of natural bone through biological principles and the processes of self-assembly or self-organization [5]. Biomimetic mineralization is a powerful approach for the synthesis of advanced scaffold materials with complex shapes, hierarchical organization and controlled size, shape and polymorphism under ambient conditions in aqueous environments.

Chitosan is partially deacetylated chitin, which is found in nature as a major organic component in several biocomposites, and has a crucial role in the hierarchical control of the biomineralization process. Furthermore, chitosan is one of the most important candidates for bone tissue engineering scaffolds, and possesses better mechanical properties than other natural polymers [6, 7]. Therefore, in this study polysaccharide chitosan scaffolds were selected as

*Corresponding author, e-mail: tcrz9@jnu.edu.cn

the porous matrix for mineralization, which control the nucleation, deposition and growth of the nanometer scaled HAP. It will be always very difficult to mimic exactly the calcification process that occurs in bone. This is further complicated by the fact that all mineralization processes are ultimately controlled by the cells directly associated to the tissue formation [8]. In literatures, nanometer scaled HAP powders and coatings can be synthesized using a number of strategies including sol-gel processing [9], co-precipitation [10, 11], emulsion techniques [12], batch hydrothermal processes [13–17], mechano-chemical methods [18] and chemical vapor deposition [19]. However, bio-compatible and environment-friendly pathway to synthesize biocomposites of HAP-biomolecule is also being explored. In this study, authors tried to prepare nanoscopic composite materials with a fast, facile and efficient way in large quantities. An ethanol-water solvent was used to control the formation, morphology and phase transition of HAP under 80ºC. Urea was utilized as a buffer reagent to balance pH value of the system, which decomposes into carbonate ion and ammonia in aqueous solution.

Such one-pot approach was easily manipulated and repeated. Furthermore, large quantity of nano HAP and mineralized scaffolds could be obtained spontaneously. The main aim of our study is not only to emulate a particular biological architecture or system, but to abstract the guiding principles and use such ideas for a broad application. Therefore, this rapid synthesis approach could also be extended to design other mineralized materials and devices.

2. Experimental section

2.1. Materials

Chitosan (MW 150,000, viscosity 200 mPas, 85% deacetylation) was obtained from Fluka Biochemical Ltd (Sigma-Aldrich Chemie GmbH, Buchs, Switzerland) and was purified before use. Hydroxyapatite (HAP, thermal spraying powder) were purchased from Plasma Biotal Limited (Buxton, UK), used as a control. Other chemicals in this study were: acetic acid, ethanol and calcium chloride from Merck GmbH (Darmstadt, Germany); sodium hydroxide from Fluka Biochemical Ltd; urea from Sigma/Aldrich Inc (Sigma-Aldrich Chemie GmbH, Buchs, Switzerland). All the chemicals were analytical reagent grade.

2.2. Preparation of chitosan scaffolds

Chitosan flakes were dissolved in 1 wt% acetic acid solution at room temperature to obtain 1.5 wt% homogeneous solution. The solution was filtered to remove air bubbles trapped in the viscous solution. Afterwards chitosan solution was cast into a polystyrene Petri dish and frozen at –80ºC for 2 h, and then freeze-dried overnight. The chitosan scaffolds (named as CS scaffolds) were washed with sodium hydroxyl/ethanol solution and 85 wt% ethanol to remove acetic acid, and then underwent a second freeze-drying.

2.3. Mineralization of CS scaffolds

CS scaffolds were placed in a wide-mouth bottle containing 0.3 g urea and 20 ml mixed solvents of ethanol and distilled water (3:1, v/v). Afterwards, a certain amount of dibasic sodium phosphate (0.1M) and calcium chloride (0.1M) with the molar ratio of 1.67 were introduced under magnetic stirring. This mixture was adjusted to become weakly alkaline by adding sodium hydroxide solution. Finally, the bottle was closed tightly and kept in the oven at 80ºC for 24 and 48 hours respectively. (The scaffolds were named as BCS-24h and BCS-48h respectively). After mineralization process, the scaffolds were washed with 85% ethanol thoroughly and were freeze-dried. The precipitation in suspension was centrifuged and washed with distilled water and dried at 60ºC for further study (named as apatite-24 h and apatite-48 h respectively).

2.4. Characterization of the scaffolds

The crystal structure of BCS scaffolds and the apatite formed in suspension were determined with a powder X-ray diffractometer (D8 X-ray diffractometer) employing the Cu–K_α line. Data were collected from 10 to 60° (2θ values), with a step size of 0.02°, and a counting time of 1 s per step. The composition of the BCS scaffolds was measured by a Fourier Transform Infrared spectrometer (FT-IR, FTS 6000 Spectrometer, Bio-RAD). Transmission electron microscopy (TEM) was used to evaluate the crystals formed in the solution and on the chitosan matrix which were achieved by ultrasonic dispersion. An environmental scanning electron microscope (ESEM, Quanta 600 FEG, FE-ESEM, FEI Europe) was employed to detect the surface topography and microstructure of the scaffolds. To ana-

lyze the mechanical property improvement of these scaffolds, the compression test was performed at room temperature using a Zwick universal testing machine (Zwick Z010, Zwick GmbH, Germany, software Testexpert V10.11). Three cubic scaffolds (dry state) were tested for each sample. Tests were conducted with a constant strain rate of 2 mm·min^{-1}, either up to failure or until 70% reduction in specimen height. The compressive modulus (E) was determined by linear regression from the slopes in the initial elastic portion of the stress-strain diagram.

3. Results and discussion

3. 1. Determination of crystalline component with XRD

Figure 1 shows the XRD patterns of the BCS scaffolds and the apatite in the suspension. The Bragg peaks observed approximately at 26, 28, 29, 30–35, 39, 46, 49, and 50º (2θ) correspond to the pure phase HAP [20], as the bar graph shows in the bottom of Figure 1. Figure 1a demonstrates that the apatite formed in the suspension was HAP but with poor crystallinity. However apatite on BCS-24h presents the characteristic peaks of HAP and dicalcium phosphate phase (DCP, marked as solid dots in Figure 1b). The non-uniformity of reaction microenvironments in bulk solution and around chitosan scaffolds surface may be responsible for this difference. Generally, the DCP is not stable in alkaline solution at chemistry laboratory [21]. HAP phase always coexisted with other calcium phosphates even in natural bone, such as DCP, TCP (tricalcium phosphate), OCP (octacalcium phosphate), amorphous phases, etc [22, 23]. After 48 h, the XRD peaks of DCP phase disappears in the chitosan composites and all sharp peaks can be indexed as pure phase of HAP with high crystallinity (Figure 1d). And the XRD pattern of apatite-48 h (Figure 1c) has no typical differences from that of apatite-24 h, wherein the broad peaks may be attributed to the small particle size and crystal lattice strains.

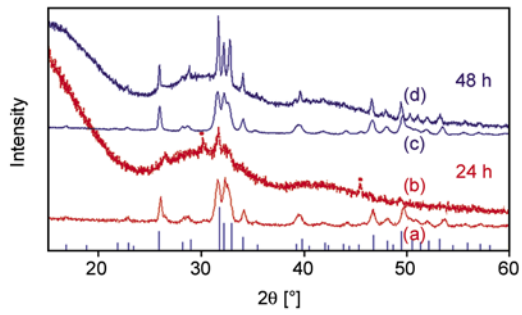

Figure 1. XRD patterns of samples: (a) apatite-24 h; (b) BCS-24h; (c) apatite-48 h and (d) BCS-48h. The bar graph at the bottom is indexed HAP peaks according to JCPDS 9-432. The solid dot marked in (b) is DCP (JCPDS 9-80).

3.2. Determination of phase composition with FT-IR

The spectra of native chitosan (see Figure 2a) exhibited the characteristic bands at 1648 cm^{-1} (amide I), 1590 cm^{-1} (amide II) and 1375 cm^{-1} (amide III). Wave number 1026 cm^{-1} was the primary amino groups (–NH_2) at C_2 position of glucosamine. Stretching of primary alcoholic groups (–CH_2OH) was at 1056 cm^{-1}. The FT-IR spectra of mineralized CS scaffolds (Figure2b and c) showed a strong band at near 1020 cm^{-1} which means that the absorption of –NH_2 and PO_4^{3-} were aligned. Furthermore it could be detected that the three characteristic signals of HAP (1089, 1018 and 961 cm^{-1}) were more intensive in BCS-48h than in BCS-24h. Figure 2d is the spectra of commercial HAP, where the three peaks were assigned as stretching vibrations of PO_4^{3-} ions.

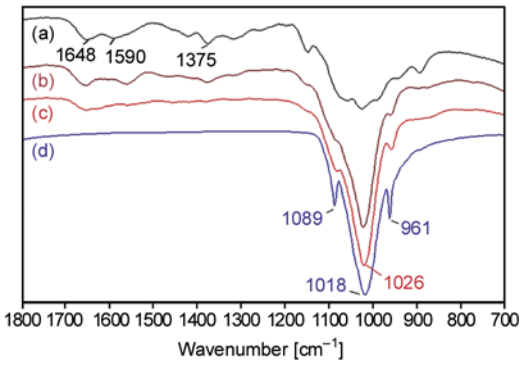

Figure 2. FT-IR spectra of samples: (a) native CS, (b) BCS-24h sponge, (c) BCS-48h sponge and (d) commercial HAP powder, Plasma Biotal Limited, UK

3.3. Morphology of the scaffolds

Figure 3a) is the image of white and soft CS scaffold, which possessed thin, smooth and porous walls. ESEM image of apatite-48 (Figure 3b) showed that the nanorods are uniform and the diameter is about 100 nm. However the apatite deposited on the chitosan scaffolds was different from that suspended in solution. From the previous reports, HAP tends to form one dimensional nanowires or sea-urchin aggre-

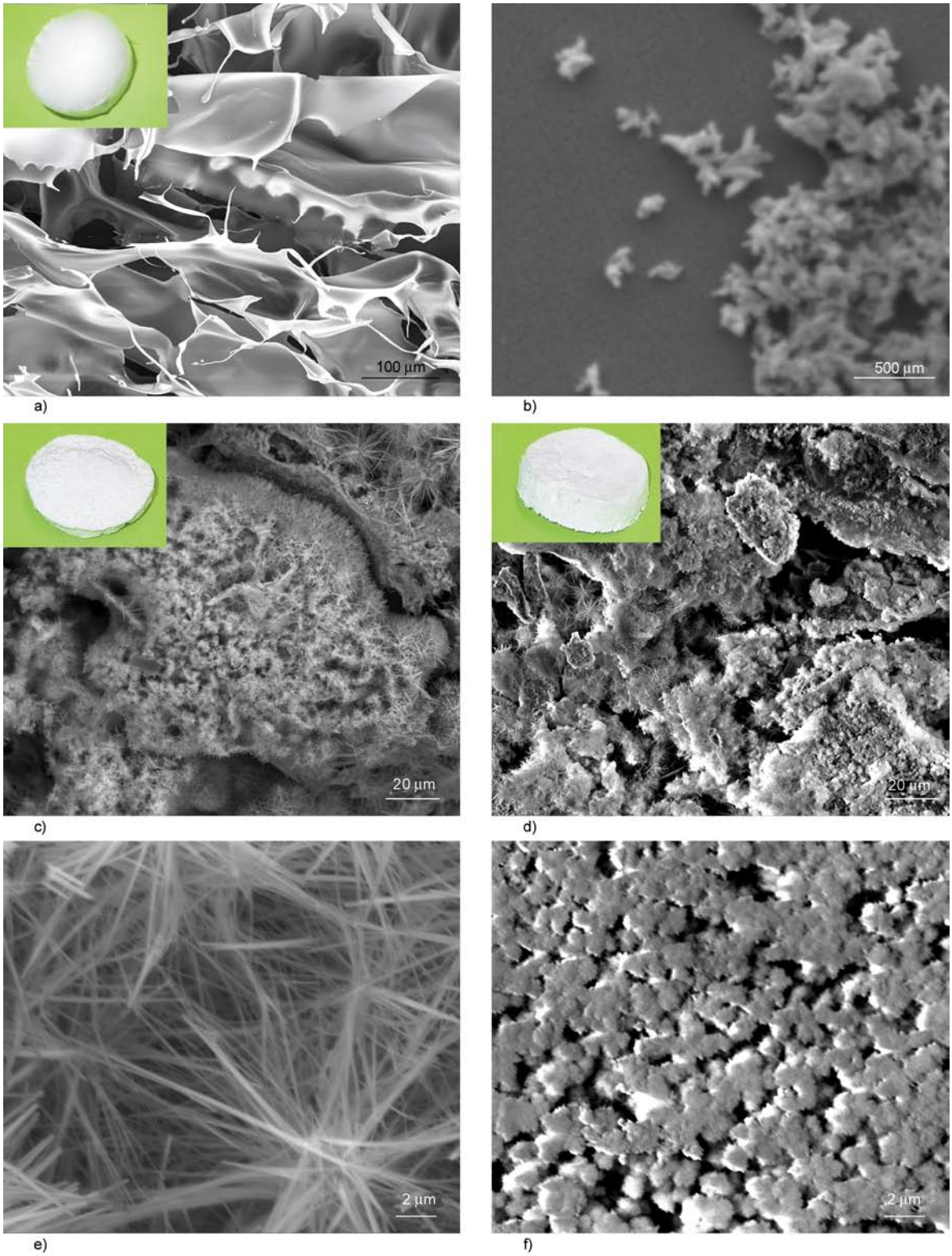

Figure 3. ESEM images of original CS sponge (a), apatite-48 h (b), BCS-24h (c), BCS-48h (d), higher magnification images of the large apatite aggregates (e) and small aggregates (f)

gates consisting of nanorods or nanowires in aqueous solution [24–26]. Here, the interesting point is the different morphologies of HAP formed in solution and on chitosan scaffolds walls. Figure 3c presents one ESEM image of the apatite deposited on the scaffolds for 24 hours (BCS-24h), which shows loose mineral layer of sea-urchin structure with different sizes. From flat areas to the pores of the

matrix, the apatite aggregates become bigger. In the pores of the scaffolds, the aggregates are more than ten times larger than that on the other areas. The HAP mineral layer becomes thicker and tighter on the BCS-48h scaffolds, as shown in Figure 3d. Similar to what happened on BCS-24h scaffolds, large amount of sea-urchin aggregates with bigger sizes in the pores, and the smaller size of the aggregates in flat areas are also visible. More details of HAP aggregates with larger size in the pores were present in Figure 3e. It demonstrates that the diameter of the sea-urchin HAP aggregates are more than 20 μm, which consist of uniform thin nanowires with a length of more than 10 μm and a diameter of less than 150 nm. And these sea-urchin like HAP structures aggregated together to form a network in the pores of the scaffolds. Small sea-urchin aggregates (diameter ca. 2 μm) made a thick deposit on the flat areas (BCS-48h, Figure 3f). Here, it is worth to note that the size of the aggregates in pores is ten times of that on the flat areas by checking most areas on the matrix during the ESEM measurement.

To check the mineralization inside the scaffolds, cryo-fractured cross sections were observed with ESEM as well. Both scaffolds (BCS-24h, 48h) showed plenty of apatite aggregation on the matrix walls (see Figure 4a and 4c). From Figure 4b, nano-sized apatite particles and some spheres adhere on the inside walls of BCS-24h. After 48 hours mineralization, HAP nanopaticles grew bigger and continuously to form a dense film covering on the BCS-48h scaffolds (Figure 4d). Moreover, the amount of micron size spheres increased and joined together. It is obvious that the HAP film became denser and thicker when the chitosan scaffolds were mineralized for 48 hours. Hence, the mineralization of HAP

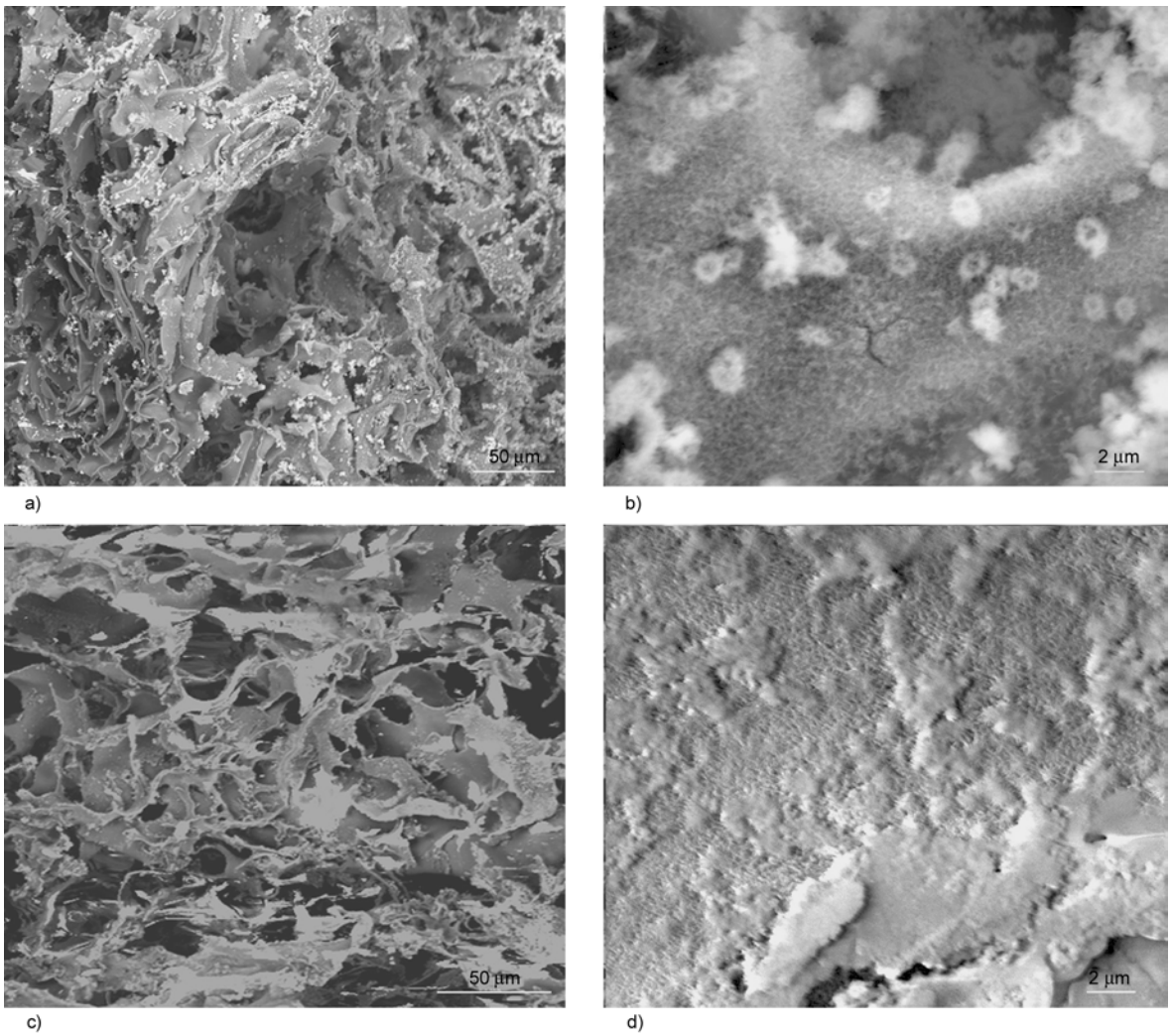

Figure 4. Cross section of the chitosan scaffolds with SEM observation. (a) and (b) BCS-24h scaffolds. (c) and (d) BCS-48 scaffolds with different magnification.

on the chitosan scaffolds is successful, which the dense mineral layer attached on the outside and inside surfaces of the scaffolds.

3.4. TEM micrographs

Transmission electron microscope (TEM) images of the apatite-48 h (Figure 5a) revealed well defined crystalline tapes of ca. 80×15 nm (aspect ratio ca. 5.5). The HAP nanorods are monodisperse and uniform in size, although there is some random aggregation of HAP nanorods. The HAP on BCS-48h scaffolds was collected with ultrasonic vibration. The TEM image demonstrates that the HAP crystals are much larger in size and aggregate into sea-urchin structure (Figure 5b). This observation is accordance with the SEM images.

3.5. Mechanical properties

In nature, bone strength depends on bone matrix volume, micro architecture, and also on the degree of mineralization. The more cancellous tissue is mineralized, the higher stiffness it is [27]. In this study we achieved similar results. The original chitosan sponges were very soft, with compressive strength of 0.09±0.012 MPa. After mineralization, the compression strength of CS scaffolds got a dramatic increase, rising to 0.54±0.005 and 0.55±0.003 MPa respectively. This increase in compression strength can be attributed to the mineralized mineral layer on the chitosan, and thicker mineral layer leads to the higher compression strength of the scaffolds (0.55 MPa, BCS-48h). Moreover, the compressive modulus of BCS-48h (29.29±1.25 MPa) is obviously higher than that of the BCS-24h (24.47±0.45 MPa), which reveals that thick nano HAP layer makes the scaffolds stiffer. Comparing with the data of human bone, the compressive strength of the composite scaffold is still far from that of cortical bone (Strength of 130–180 MPa, modulus of $12–18 \cdot 10^3$ MPa) and cancellous bone (Strength of 4–12 MPa, modulus of $0.1–0.5 \cdot 10^3$ MPa) [28–30], but closer to cartilage (Strength of 4–59 MPa and modulus of 1.9–14.4 MPa [31, 32] or initial soft callus which has modulus closer to 1 MPa. Therefore these materials can be suggested to be used as substitute for cartilage, non-load-bearing bone or initial fracture healing callus substitute, which can remodel and develop into bone tissue.

3.6. Mechanism of mineralization

One of the fundamental aspects controlling the final habit of a growing crystal is the balance between kinetic and thermodynamic control, which plays a key role in crystal growth, determines the final crystal habit, phase, shape, and structure [33, 34]. The precipitation of calcium phosphate from aqueous solution is somewhat complicated due to the possible occurrence of several different calcium phosphates with or without hydrogen/hydroxide group, depending on the solution composition and the pH value [35–37]. These phosphates salts include dicalcium phosphate (DCP), dicalcium phosphate dehydrate (DCPD), tricalcium phosphate

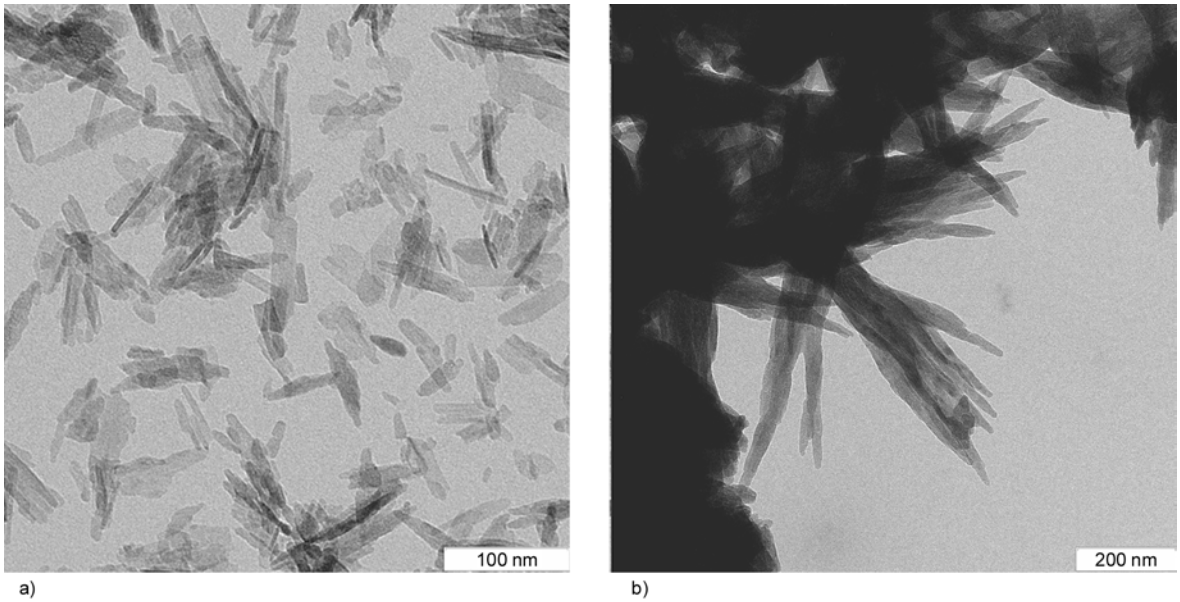

Figure 5. Transmission electron micrographs of hydroxyapatite: (a) apatite-48h and (b) apatite on the BCS-48h scaffolds

(TCP), octacalcium phosphate (OCP), HAP, amorphous calcium phosphate (ACP), and so on [38, 39]. However, HAP phase is more stable than other salts stated above in alkaline aqueous. Hence, some people report that these phosphate salts were used as precursor for preparation of HAP or were observed as transitory by-products in their experiments [21, 40]. In this work, DCP were characterized at the early stage of reaction, which can be regarded as transition phase or precursor. At 80°C, urea decomposed into CO_2 and NH_3, then dissolved in aqueous solution and hydrolyzed to HCO_3^- or CO_3^{2-} and NH_4^+ in solution. These ions kept the solution weakly alkaline for the slow hydrolysis of DCP and crystallization of HAP. The mechanics of the mineralization in this study was analyzed as following.

Crystallization in bulk solution and on chitosan surface

The spatially periodic functional groups $-NH_3^+$ on the surface of the CS substrate interacted with the phosphate anions when the dibasic sodium phosphate solution was introduced into the wide mouth bottle containing urea mixed solvents and CS. Here, it should be noted that one part of the phosphate anions would be stabilized by the $-NH_3^+$ group of CS and the other part of free phosphate anions would stay in bulk solution, as shown in the scheme (Figure 6a and 6b). Then DCP phase formed on CS surface or in bulk solution when the calcium chloride solution was introduced into the bottle by the reaction between the hydrogen phosphate and calcium (Figure 6c). However, the salt was not stable in alkaline solution and especially at 80°C. Then, the hydrolysis was carried on for the formation of the thermodynamic stable HAP phase (Figure 6d) [41]. During the hydrolysis of DCP phase for formation of HAP phase, the free cations and anions in bulk solution crystallized homogenously to form uniform HAP nanorods (Figure3b and 5a). Considering the strong binding between the phosphate ions and CS, it is reasonable to assume that hydrolysis of the DCP on the CS would slow down. With the comparison of XRD patterns of BCS-24h and apatite-24h (Figure 1a and b), it is found that DCP phase is still resident on the CS surface after even 24 hours reaction (Figure 1b), while all of powders suspended in bulk solution were characterized as pure phase of HAP (Figure 1a). In one previous paper for elucidate the residue of DCP phase, the author found that the formation of HAP and the hydrolysis of DCP were competitive [41]. But, in this work, this viewpoint can not be interpreted completely why DCP phase was only resident on the CS surface and no DCP phase mixed in powders outside of the scaffolds. Hence, this phenomenon proved laterally that the DCP crystallized at the interface of phosphate-chitosan, and the interface can stabilize the meta-stable DCP phase for a long time. Moreover, the stabilization of DCP precursor

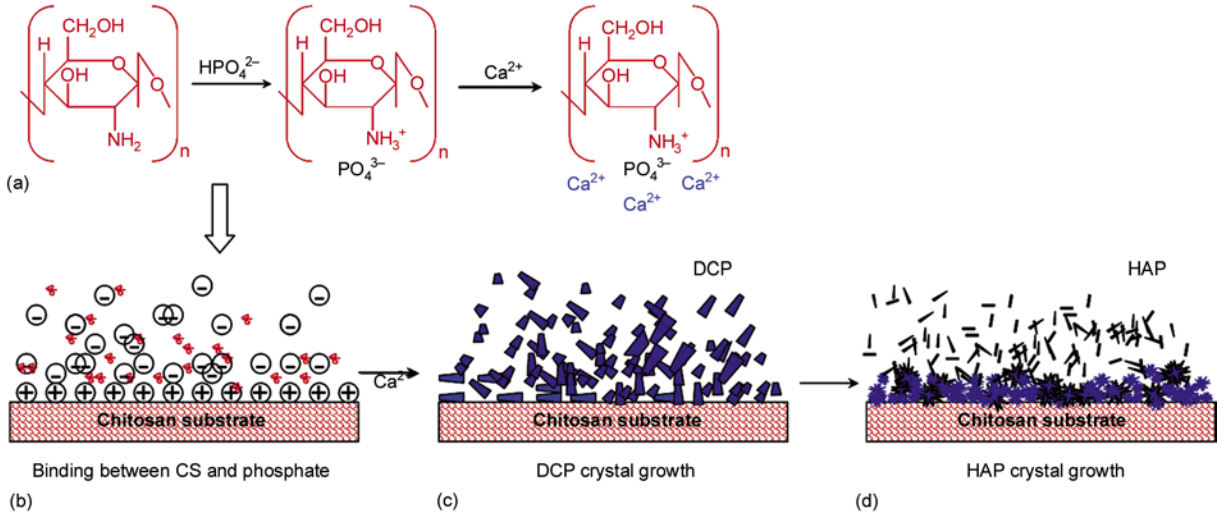

Figure 6. Schematic illustration of the major steps involved in the mineralization on chitosan matrix. (a) a scheme of chitosan molecule role in the mineralization of CS matrix, and scheme of chitosan sponge substrate mineralization: (b) Strong interaction between CS and phosphate, which facilitates the nucleation of crystals. (c) Colloidal cloud of amorphous calcium phosphate forms after addition of Ca^{2+} ions (formation of DCP phase after addition of Ca^{2+} ions) and (d) HAP crystals grow on the substrate.

changed kinetic factors of crystallization of HAP to some extent, leading to the different morphology on the CS surface.

Mechanism of chitosan-HAP bio-composite film

The strong binding of phosphate anions with the positive charge on the chitosan (a linear polysaccharide) will induce a high supersaturation degree near to the chitosan. And this binding was functioned for nucleating DCP firstly (Figure 6c) and then HAP secondly (Figure 6d) by hydrolysis of DCP. As stated above, the $-NH_3^+$ group is periodically arranged in the CS. The nucleuses of HAP were bound by the $-NH_3^+$ group protruding on the CS and covered the scaffolds surface in the process of DCP hydrolysis. The covering of HAP nucleuses on the scaffolds should be responsible for the formation of HAP film and the HAP-biocomposites. Moreover, it was reported that CS bound preferentially to the (100) face of the HAP crystal [42]. So, the HAP nuclei then grew out of CS surface along the c-axis by the Oswald-ripening mechanism [43]. With the time extension, HAP nano crystals grew bigger, and the mineral film become denser and thicker by the hydrolysis of DCP residue, which can be observed from Figure 3c–d.

The similar process also happened in the inside surface of CS. Crystals on the cross section of CS (Figure 4b, 4d) were much smaller than that on the outer surface (Figure3c–f), because the outer surface was surrounded by bulk reaction solution and inside surface of scaffolds not. For the inside surface of CS, the nuclei of HAP were also bound by the positive charge, and then grew bigger by hydrolysis of DCP. But the concentration of cations and anions inside of CS were lower than that in bulk solution, so the HAP crystal was smaller. But, the mineral layer became thicker and denser when the reaction time elongated to 2 days (Figure 4). In a word, the HAP layer covered both outside and inside the surface of CS. It is found that the chitosan improved the crystalline quality of HAP phase which grew on CS (Figure 1c–d), although the exact reason is not clear now.

Mechanical properties of the biocomposites

The mineral layer deposited on the CS scaffolds greatly improved the mechanical properties. In biomineralized tissues such as bone, the recurring structural motif at the supramolecular level is an anisotropic stiff inorganic component reinforcing the soft organic matrix. There would be two aspects to improve the mechanical properties of the composite. The stiff nano HAP crystals covered on the surface of CS film and filled in the micropores of the CS scaffolds, which increased the hardness of the chitosan matrix. At the same time, thick mineral layer limited the conformation of the CS during compression, redistributed effectively the strain energy within materials and improve the toughness [44]. With the elongation of mineralization time, the mineral layer became thicker (Figure 4), therefore composites became stiffer and tougher, resulting in higher compression strength and modulus.

4. Conclusions

In a summary, biomimetic mineralization of CS scaffolds was performed successfully in a rapid and efficient approach. HAP crystals formed in scaffolds possessed higher crystallinity than that in solution. HAP mineral layer densely covered CS both outside and inside surfaces. Moreover, the mineralized HAP layer increased the mechanical properties of HAP-CS bio-composites. A mechanism was proposed to elucidate the formation, and the effects of CS on the nucleation of HAP were analyzed not only from the viewpoint of nucleation kinetics but also from the viewpoint of a molecular level. We can foresee that the one-pot process to form large quantities of mineralized materials and nano HAP. Further work is underway to study the properties of the 3D porous hybrid materials.

Acknowledgements

The work was supported by the National HighTechnology Research and Development Program of China (‘863’ Program, 2007AA091603). Li L.H. thanks for the financial support by the MPIKG and DAAD exchange fellowship of Germany.

References

[1] Elliot J.: Structure and chemistry of the apatites, and other calcium orthophosphates. Elsevier, Amsterdam (1994).

[2] Webster T., Ergun C., Doremus R., Siegel R., Bizios R.: Enhanced functions of osteoblasts on nanophase ceramics. Biomaterials, **21**, 1803–1810 (2000). DOI: 10.1016/S0142-9612(00)00075-2

[3] Alves N. M., Leonor I. B., Azevedo H. S., Reis R. L., Mano J. F.: Designing biomaterials based on biomineralization of bone. Journal of Materials Chemistry, **20**, 2911–2921 (2010).
DOI: 10.1039/B910960A

[4] Green D., Walsh D., Mann S., Oreffo R.: The potential of biomimesis in bone tissue engineering: Lessons from the design and synthesis of invertebrate skeletons. Bone, **30**, 810–815 (2002).
DOI: 10.1016/S8756-3282(02)00727-5

[5] Li Q-L., Chen Z-Q., Dawell B. W., Zeng Q., Li G., Ou G-M., Wu M-Y.: Biomimetic synthesis of the composites of hydroxyapatite and chitosan–phosphorylated chitosan polyelectrolyte complex. Materials Letters, **60**, 3533–3536 (2006).
DOI: 10.1016/j.matlet.2006.03.046

[6] Li L. H., Kommareddy K. P., Pilz C., Zhou C. R., Fratzl P., Manjubala I.: In vitro bioactivity of bioresorbable porous polymeric scaffolds incorporating hydroxyapatite microspheres. Acta Biomaterialia, **6**, 2525–2531 (2010).
DOI: 10.1016/j.actbio.2009.03.028

[7] Di Martino A., Sittinger M., Risbud M.: Chitosan: A versatile biopolymer for orthopaedic tissue-engineering. Biomaterials, **26**, 5983–5990 (2005).
DOI: 10.1016/j.biomaterials.2005.03.016

[8] Simkiss K., Wilbur K. M.: Biomineralization. Cell biology and mineral deposition. Academic Press, San Diego (1989).

[9] Bigi A., Boanini E., Panzavolta S., Roveri N., Rubin K.: Bonelike apatite growth on hydroxyapatite-gelatin scaffolds from simulated body fluid. Journal of Biomedical Materials Research, **59**, 709–714 (2002).
DOI: 10.1002/jbm.10045

[10] Pang Y., Bao X.: Influence of temperature, ripening time and calcination on the morphology and crystallinity of hydroxyapatite nanoparticles. Journal of the European Ceramics Society, **23**, 1697–1704 (2003).
DOI: 10.1016/S0955-2219(02)00413-2

[11] Phillips M., Darr J., Luklinska Z., Rehman I.: Synthesis and characterization of nano-biomaterials with potential osteological applications. Journal of Materials Science: Materials in Medicine, **14**, 875–882 (2003).
DOI: 10.1023/A:1025682626383

[12] Lim G., Wang J., Ng S., Chew C., Gan L.: Processing of hydroxyapatite via microemulsion and emulsion routes. Biomaterials, **18**, 1433–1439 (1997).
DOI: 10.1016/S0142-9612(97)00081-1

[13] Kothapalli C., Wei M., LeGeros R., Shaw M.: Influence of temperature and aging time on HA synthesized by the hydrothermal method. Journal of Materials Science: Materials in Medicine, **16**, 441–446 (2005).
DOI: 10.1007/s10856-005-6984-5

[14] Wang Y., Zhang S., Wei K., Zhao N., Chen J., Wang X.: Hydrothermal synthesis of hydroxyapatite nanopowders using cationic surfactant as a template. Materials Letters, **60**, 1484–1487 (2006).
DOI: 10.1016/j.matlet.2005.11.053

[15] Riman R., Suchanek W., Byrappa K., Chen C-W., Shuk P., Oakes C.: Solution synthesis of hydroxyapatite designer particulates. Solid State Ionics, **151**, 393–402 (2002).
DOI: 10.1016/S0167-2738(02)00545-3

[16] Zhang F., Zhou Z-H., Yang S-P., Mao L-H., Chen H-M., Yu X-B.: Hydrothermal synthesis of hydroxyapatite nanorods in the presence of anionic starburst dendrimer. Materials Letters, **59**, 1422–1425 (2005).
DOI: 10.1016/j.matlet.2004.11.058

[17] Liu J., Ye X., Wang H., Zhu M., Wang B., Yan H.: The influence of pH and temperature on the morphology of hydroxyapatite synthesized by hydrothermal method. Ceramics International, **29**, 629–633 (2003).
DOI: 10.1016/S0272-8842(02)00210-9

[18] Rhee S-H.: Synthesis of hydroxyapatite via mechanochemical treatment. Biomaterials, **23**, 1147–1152 (2002).
DOI: 10.1016/S0142-9612(01)00229-0

[19] Darr J., Guo Z., Raman V., Bououdina M., Rehman I.: Metal organic chemical vapour deposition (MOCVD) of bone mineral like carbonated hydroxyapatite coatings. Chemistry Communication, **6**, 696–697 (2004).
DOI: 10.1039/b312855p

[20] Danilchenko S., Koropov A., Sulkio-Cleff B., Sukhodub L.: Thermal behavior of biogenic apatite crystals in bone: An X-ray diffraction study. Crystal Research Technology, **41**, 268–275 (2006).
DOI: 10.1002/crat.200510572

[21] Ito H., Oaki Y., Imai H.: Selective synthesis of various nanoscale morphologies of hydroxyapatite via an intermediate phase. Crystal Growth and Design, **8**, 1055–1059 (2008).
DOI: 10.1021/cg070443f

[22] Newman W., Newman M.: The chemical dynamics of bone mineral. The University of Chicago Press, Chicago (1958).

[23] González M., Hernández E., Ascencio J., Pacheco F., Pacheco S., Rodríguez R.: Hydroxyapatite crystals grown on a cellulose matrix using titanium alkoxide as a coupling agent. Journal of Materials Chemistry, **13**, 2948–2951 (2003).
DOI: 10.1039/b306846n

[24] Chen J. D., Wang Y. Y., Wei K., Zhang S. H., Shi X. T.: Self-organization of hydroxyapatite nanorods through oriented attachment. Biomaterials, **28**, 2275–2280 (2007).
DOI: 10.1016/j.biomaterials.2007.01.033

[25] Huang F., Shen Y., Xie A., Zhu J., Zhang C., Li S.: Study on synthesis and properties of hydroxyapatite nanorods and its complex containing biopolymer. Journal of Materials Science, **42**, 8599–8605 (2007).
DOI: 10.1007/s10853-007-1861-x

[26] Choi A., Ben-Nissan B.: Sol-gel production of bioactive nanocoatings for medical applications. Part II: current research and development. Nanomedicine, **2**, 51–61 (2007).
DOI: 10.2217/17435889.2.1.51

[27] Follet H., Boivin G., Rumelhart C., Meunier P.: The degree of mineralization is a determinant of bone strength: A study on human calcanei. Bone, **34**, 783–789 (2004).
DOI: 10.1016/j.bone.2003.12.012

[28] Kerin A., Wisnom M., Adams M.: The compressive strength of articular cartilage. Journal of Engineering in Medicine, **212**, 273–280 (1998).

[29] Seal B., Otero T., Panitch A.: Polymeric biomaterials for tissue and organ regeneration. Materials Science and Engineering R: Reports, **34**, 147–230 (2001).
DOI: 10.1016/S0927-796X(01)00035-3

[30] Keaveny T., Hayes W.: Mechanical properties of cortical and trabecular bone. in 'Bone, Volume VII: A Treatise' (ed.: Hall B. K.) CRC press, Boca Raton, 285–344 (1993).

[31] Zioupos P., Currey J.: Changes in the stiffness, strength, and toughness of human cortical bone with age. Bone, **22**, 57–66 (1998).
DOI: 10.1016/S8756-3282(97)00228-7

[32] Qiu G., Mei X., Hong Z.: The development of artificial articular cartilage–PVA-hydrogel. Bio-Medical Materials and Engineering, **8**, 75–81 (1998).

[33] Cölfen H., Mann S.: Higher-order organization by mesoscale self-assembly and transformation of hybrid nanostructures. Angewandte Chemie International Edition, **42**, 2350–2365 (2003).
DOI: 10.1002/anie.200200562

[34] Chen S., Yu S-H., Yu B., Ren L., Yao W., Cölfen H.: Solvent effect on mineral modification: Selective synthesis of cerium compounds by a facile solution route. Chemistry – A European Journal, **10**, 3050–3058 (2004).
DOI: 10.1002/chem.200306066

[35] Gouveia D. S., Bressiani A. H. A., Bressiani J. C.: Phosphoric acid rate addition effect in the hydroxyapatite synthesis by neutralization method. Materials Science Forum, **530–531**, 593–598 (2006).
DOI: 10.4028/www.scientific.net/MSF.530-531.593

[36] Liu C., Huang Y., Shen W., Cui J.: Kinetics of hydroxyapatite precipitation at pH 10 to 11. Biomaterials, **22**, 301–306 (2001).
DOI: 10.1016/S0142-9612(00)00166-6

[37] Inskeep W., Silvertooth J.: Kinetics of hydroxyapatite precipitation at pH 7.4 to 8.4. Geochimica et Cosmochimica Acta, **52**, 1883–1893 (1988).
DOI: 10.1016/0016-7037(88)90012-9

[38] Suzuki O.: Interface of synthetic inorganic biomaterials and bone regeneration. International Congress Series, **1284**, 274–283 (2005).
DOI: 10.1016/j.ics.2005.06.066

[39] Rudin V., Komarov V., Melikhov I., Minaev V., Orlov A., Bozhevolnov V.: Method for producing nano-sized crystalline hydroxyapatite. U.S. Patent 7169372, USA (2007).

[40] Moon P., Sandí G., Stevens D., Kizilel R.: Computational modeling of ionic transport in continuous and batch electrodialysis. Journal of Materials Science, **39**, 2531–2555 (2004).
DOI: 10.1081/SS-200026714

[41] Fulmer M., Brown P.: Hydrolysis of dicalcium phosphate dihydrate to hydroxyapatite. Materials Science: Materials in Medicine, **9**, 197–202 (1998).
DOI: 10.1023/A:1008832006277

[42] Jiang H., Liu X-Y., Zhang G., Li Y.: Kinetics and template nucleation of self-assembled hydroxyapatite nanocrystallites by chondroitin sulfate. The Journal of Biological Chemistry, **280**, 42061–42065 (2005).

[43] Liu X.: Generic mechanism of heterogeneous nucleation and molecular interfacial effects. in 'Advances in crystal growth research' (ed.: Saito K.) Elsevier, Amsterdam, 42–61 (2001).

[44] Gupta H., Seto J., Wagermaier W., Zaslansky P., Boesecke P., Fratzl P.: Cooperative deformation of mineral and collagen in bone at the nanoscale. PNAS, **103**, 17741–17746 (2006).
DOI: 10.1073/pnas.0604237103